IOP Conf. Series: Materials Science and Engineering **1344** (2026) 012145 doi:10.1088/1757-899X/1344/1/012145

Study on Helium Adsorption Properties of Carbon Nanotubes in the Liquid Helium Temperature Range Based on the Monte Carlo Method

Zhijian Zhang [1, 2], Biao Yang [1, 2], Xiaotong Xi [3], Yihan Tian [1, 2], Zhaozhao Gao [1, 2, 4], Liubiao Chen [1, 2, 4, *], Junjie Wang [1, 2]

[1] State Key Laboratory of Cryogenic Science and Technology, Technical Institute of Physics and Chemistry, Chinese Academy of Sciences, Beijing 100190, China

[2] University of Chinese Academy of Sciences, Beijing 100049, China

[3] Tianjin Key Laboratory of Refrigeration Technology, Tianjin University of Commerce, Tianjin 300134, China

[4] Institute of Optical Physics and Engineering Technology, Qilu Zhongke, Licheng District, Jinan 250100, China

*E-mail: chenliubiao@mail.ipc.ac.cn

Abstract. The sorption pump is a key component of helium sorption cryocoolers operating in the liquid helium temperature range, where performance is strongly influenced by the adsorption properties of the porous materials used. Most studies have focused on activated carbon, while alternative porous materials such as carbon nanotubes (CNTs) remain less explored. Their helium adsorption capacity is still unclear due to differences in elemental composition, molecular structure, and surface characteristics. In this study, a molecular model of single-walled CNTs was established, and grand canonical Monte Carlo simulations were carried out to evaluate the adsorption capacity of helium-4. The calculations covered a pressure range of 1 to 200 kPa and a temperature range of 4 to 70 K, representative of cryogenic operating conditions. The results reveal distinct adsorption behaviors of helium in CNTs, with adsorption strongly dependent on pressure and temperature. These findings provide guidance for optimizing sorption pump materials and suggest that CNTs have potential as alternative sorbents in helium sorption cryocoolers.

1. Introduction

Adsorption coolers are a commonly used cryogenic cooling technology capable of achieving temperatures below 1 K and are widely applied in aerospace exploration[1]. Compared with other ultra-low temperature cooling methods, adsorption refrigeration offers advantages such as compact size, absence of vibration, and immunity to magnetic field interference. The system has a simple structure, mainly consisting of two components: an adsorption pump filled with porous materials and an evaporation chamber containing liquid helium. These two parts form a closed system connected by a pump tube. During operation, the porous material physically adsorbs helium gas from the system, thereby reducing the system pressure. Liquid helium evaporates to maintain phase equilibrium, and the evaporation process generates the cooling effect. Therefore, the helium adsorption capacity of the porous material is a critical parameter influencing the performance of the adsorption refrigerator. Various wood-based activated carbons are commonly used as porous materials in adsorption pumps[2] [3]. The adsorption characteristics of activated carbon have been extensively studied[4]. With the advancement of science and technology, carbon nanotubes (CNTs), which feature unique structures and high specific surface areas, are becoming increasingly prevalent. Compared to activated carbon, CNTs exhibit more ordered pore structures and tunable surface chemistry, making them increasingly attractive in adsorption applications.

Content from this work may be used under the terms of the Creative Commons Attribution 4.0 licence. Any further distribution of this work must maintain attribution to the author(s) and the title of the work, journal citation and DOI.
Published under licence by IOP Publishing Ltd

However, studies on the adsorption properties of helium on CNTs at cryogenic temperatures remain limited, which restricts their potential application in adsorption refrigerators.

The development of computational techniques has provided tools for analyzing material structures and behaviors at the molecular level. For example, Luis et al. used grand canonical Monte Carlo (GCMC) simulations to investigate the hydrogen adsorption capacity of various graphene models and established relationships between adsorption capacity, pore size, and number of layers[5]. Sha et al. built a model of single-walled carbon nanotube bundles and studied their selective adsorption behavior for noble gas mixtures under different pressures and mixing ratios[6]. Li et al. developed four different activated carbon models and, based on simulation results, analyzed structural features suitable for benzene adsorption at different temperatures[7]. Karki et al. compared the hydrogen adsorption properties of defective graphene and single-walled carbon nanotubes at 80 K to 298 K and pressures ranging from 1 to 500 bar[8]. These studies indicate a current lack of investigation into the adsorption behavior of ^{4}He on CNTs. In this work, a model of armchair-type single-walled carbon nanotubes is established, and adsorption isotherm of ^{4}He at several representative cryogenic temperature ranges are simulated. The simulation results provide design guidance and data support for the optimization of adsorption pumps in helium adsorption coolers, thereby improving research efficiency.

2. Model construction

After more than three decades of development, CNTs have evolved into various product types. They can be classified by the number of walls into single-walled carbon nanotubes (SWCNTs) and multi-walled carbon nanotubes (MWCNTs), and by their atomic structure into armchair, zigzag, and chiral types. The most critical structural parameter for constructing CNT models is the chiral index (n, m), which directly determines the geometry of the nanotube. In this study, models of armchair-type SWCNTs with different diameters were constructed using Materials Studio (MS) software. The basic structural unit used is shown in Figure 1. The chiral indices of the models are (6,6), (8,8), and (12,12), corresponding to diameters of 8.14 Å, 10.85 Å, and 16.27 Å, respectively.

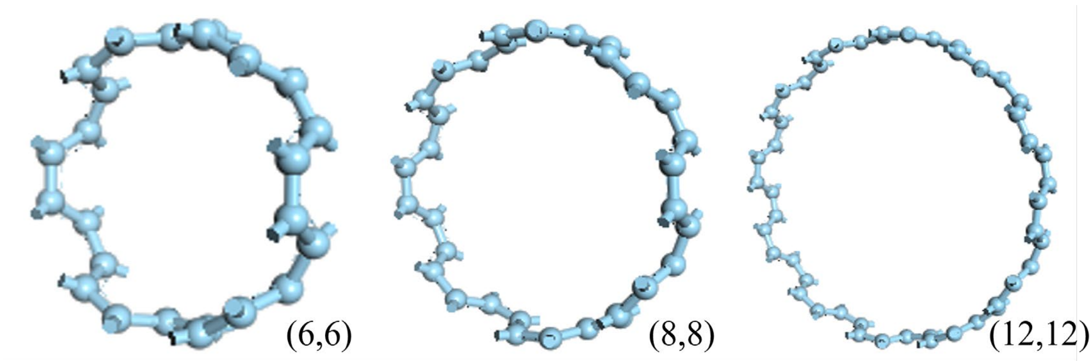

Figure 1. The units of different SWCNTs

A 3×3 supercell of SWCNTs was constructed using the three basic structural units described above, each with different inter-tube spacings. Part of models are shown in Figure 2. The lengths of the three cell edges, A, B, and C, are nearly equal. For example, for the SWCNT (6,6) with an inter-tube spacing of 3 Å, the resulting supercell dimensions are 33.4 × 33.4 × 33.4 Å. A supercell was chosen over an isolated nanotube model because it more accurately represents the structure

IOP Conf. Series: Materials Science and Engineering **1344** (2026) 012145 doi:10.1088/1757-899X/1344/1/012145

of real materials. The supercell model, with periodic boundary conditions, simulates an infinite array of carbon nanotubes and takes into account inter-tube interactions, which influence the distribution of adsorption sites and help reduce errors associated with isolated models. Additionally, the supercell approach mitigates size effects caused by short nanotube models that may introduce non-physical adsorption sites. Most importantly, the supercell model allows for tuning the inter-tube spacing, thereby enabling the simulation of porous structures with different packing densities. This makes it possible to more closely approximate experimentally measured specific surface areas and pore size distributions.

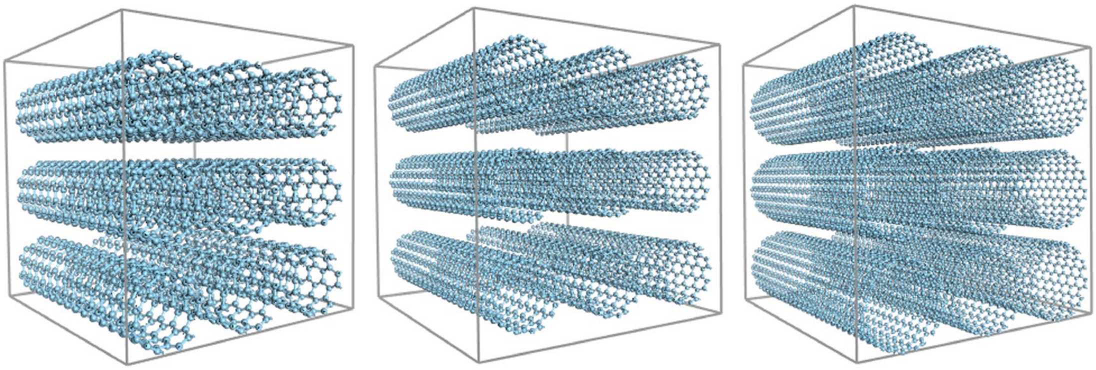

Figure 2. The structures of SWCNTs

The Atom Volume & Surface module in MS can be used to obtain data on the specific surface area (SSA) and pore volume of SWCNT molecular models. A nitrogen probe (1.84 Å in diameter) was employed to evaluate the Connolly surface parameters of the SWCNTs. In Figure 3, the red regions represent the free (accessible) volume, while the blue regions correspond to the carbon atoms.

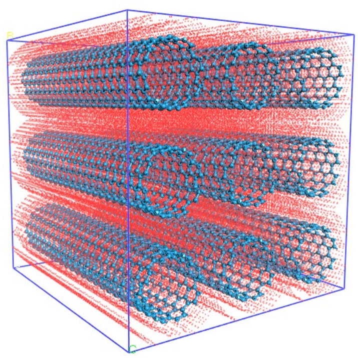

Figure 3. Free volume distribution of SWCNTs

Structural parameters such as specific surface area and pore volume can also be calculated using Equations (1) - (3), based on the nitrogen probe measurements along with the density and volume of the supercell.

$$Specific\ Surface\ Area = \frac{Surface\ Area\ per\ Cell}{Density \times Cell\ Volume} \times 10^4 \tag{1}$$

$$Pore\ Volume = \frac{Cell\ Free\ Volume}{Density \times Cell\ Volume} \tag{2}$$

$$Porosity = \frac{Cell\ Free\ Volume}{Cell\ Volume} \times 100\% \tag{3}$$

To investigate the molecular structure of SWCNTs, 3×3 supercells were constructed for each of the three chiral indices. For each chiral type, three inter-tube spacings of 3 Å, 6 Å, and 9 Å were considered. Densities and volumes for different diameters and inter-tube spacings are summarized in Table 1.

Table 1. Structure parameters of SWCNTs model

Model parameter		Density(g/cm^3)	Volume(Å^3)
	3	1.568	38474
(6,6)	6	0.973	75262
	9	0.662	136598
	3	1.354	72118
(8,8)	6	0.915	131882
	9	0.659	209193
	3	1.047	197453
(12,12)	6	0.785	296500
	9	0.61	438184

The comparative curves are shown in Figure 4. As observed from the figures, the SSA, pore volume, and porosity all increase with increasing inter-tube spacing. Additionally, the differences among nanotubes with different chiral indices gradually diminish. This is because, at smaller inter-tube spacings, parts of the nanotube surface are obstructed by adjacent tubes. As the spacing increases, previously blocked surfaces become exposed, allowing more of the outer tube walls to participate in adsorption, thereby increasing the specific surface area.

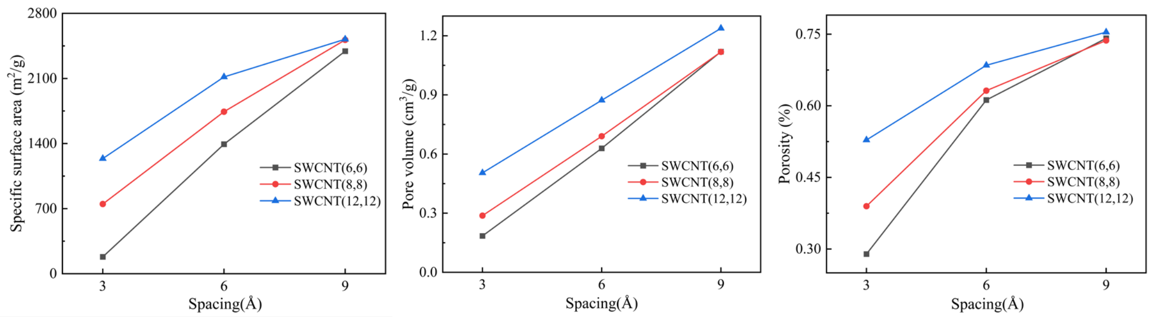

Figure 4. Structure parameters of SWCNTs with different spacings. (a)SSA. (b)Pore volume. (c)Porosity

Furthermore, as the inter-tube spacing increases, the packing density of the nanotube array decreases, leading to a significant rise in both porosity and pore volume. Among the three types, the SWCNT with the largest diameter, (12,12), consistently exhibits the highest values of specific surface area, pore volume, and porosity. When the spacing is small, a larger tube diameter results in a lower proportion of contact area between adjacent nanotubes, thus yielding a higher specific surface area for the supercell. In contrast, nanotubes with smaller diameters form narrower interstitial spaces, resulting in lower pore volume and porosity. As the diameter increases, these interstitial gaps expand, forming larger interconnected mesopores, which significantly enhances the pore volume and porosity.

3. Simulation setup

The Sorption module in Materials Studio was used to obtain data such as adsorption isotherms through the GCMC simulation method. The simulation model was defined as a 3×3 SWCNT supercell with dimensions of 48.6 × 48.6 × 49 Å and an inter-tube spacing of 5.4 Å. This model exhibited a specific surface area of 1450.7 m^2/g, which is close to the experimentally measured BET (Brunauer-Emmett-Teller) surface area of the purchased SWCNT sample (1359.1 m^2/g), while also maintaining relatively high porosity and pore volume.

A forcefield is a mathematical function used to describe the potential energy between particles and serves as the computational foundation for Monte Carlo molecular simulations. The accuracy of simulation results is strongly influenced by the choice of force field. The Sorption module includes several built-in force fields such as UFF (Universal Force Field), Dreiding, and COMPASS (Condensed-phase Optimized Molecular Potentials for Atomistic Simulation Studies). Among them, the COMPASS force field is the first to unify the treatment of both organic and inorganic systems. It is suitable for a wide range of materials, including polymers and inorganic compounds, and is widely used in materials science simulations. However, it does not support biomolecules. In this study, the COMPASS force field was selected for simulating helium adsorption. For helium, a chemically inert gas, van der Waals interactions dominate the intermolecular forces. These interactions are typically described by the Lennard-Jones (L-J) potential, and the expression for the L-J potential in the COMPASS force field is provided in Equation (4).

$$E_{vdW} = \sum_{i<j} \epsilon_{ij}[2(\frac{r_{0,ij}}{r_{ij}})^9 - 3(\frac{r_{0,ij}}{r_{ij}})^6] \tag{4}$$

Where E_{vdW} represents the total van der Waals interaction energy. ϵ_{ij} denotes the maximum attractive energy between atoms i and j, $r_{0,ij}$ is the distance at which the potential energy is zero (also known as the equilibrium distance), r_{ij} is the actual distance between atoms i and j.

In addition to the choice of force field, the adsorption simulation was performed using the Metropolis algorithm as the sampling method. The simulation temperatures and fugacities were set accordingly, with fugacity values obtained from the NIST database. Because the operating pressure of the adsorption pump in helium adsorption refrigerators is generally below 200 kPa, the selected simulation pressures were 1, 10, 50, 100, and 200 kPa. The simulation temperatures were selected to represent typical points within the temperature range between liquid helium and liquid nitrogen, specifically: 4, 6, 10, 20, 45, and 77 K. At 4 K, the saturation pressure of ^4He is approximately 80 kPa, so the maximum simulation pressure at this temperature was set to 80 kPa. The total number of Monte Carlo steps was set to 550,000, including both equilibration and production steps.

4. Result Discussion

The simulation results for the helium adsorption capacity are shown in Figure 5. It can be observed that, at the same temperature, the adsorbed amount increases with increasing pressure. This is because higher pressure leads to a higher collision frequency between helium atoms and the surface of the SWCNTs, allowing more helium atoms to be captured by adsorption sites. At lower temperatures, adsorption reaches saturation at lower pressures. For instance, at 4 K and 6 K, the adsorption amount remains nearly constant across the entire pressure range studied, indicating that saturation has already been achieved. In contrast, at 10 K, the system reaches saturation at about 100 kPa. At higher temperatures such as 45 K and 77 K, the adsorption isotherms show a more gradual increase, and at 77 K, the adsorbed amount at 200 kPa is still less than 1 mmol/g, indicating minimal adsorption.

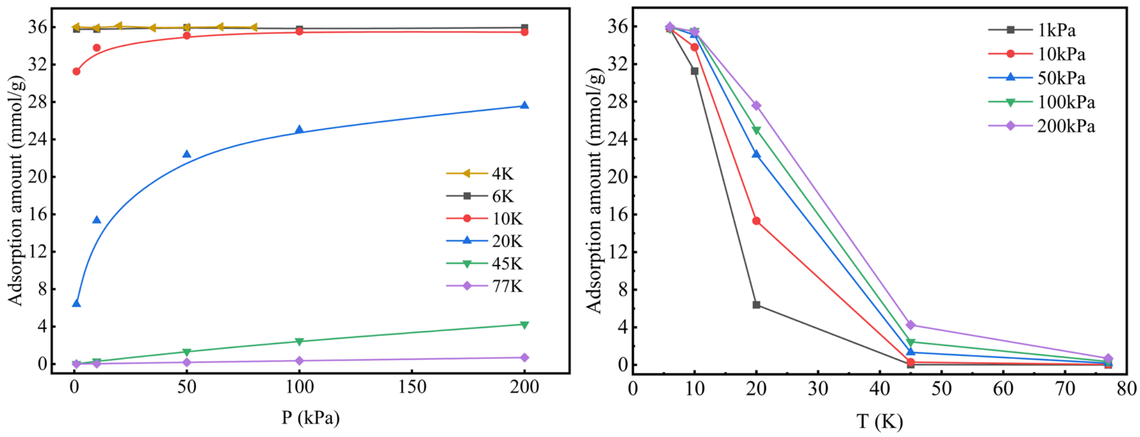

Figure 5. Variation in adsorption capacity of SWCNTs with (a) pressure and (b) temperature.

At the same pressure, the results demonstrate that SWCNTs exhibit stronger adsorption capacity at lower temperatures. This is because gas adsorption is an exothermic process, and at low temperatures, the kinetic energy of helium atoms is reduced, making it easier for them to be trapped in the van der Waals potential wells of the nanotube surface. The difference in adsorption capacity across temperatures is significant. At 4 K, the maximum adsorption amount reaches 36.14 mmol/g, while at 45 K, the maximum is only 4.25 mmol/g. At the same pressure, lower temperatures consistently lead to higher adsorption capacities. Moreover, this temperature dependence becomes more pronounced at lower pressures. For example, at 1 kPa, increasing the temperature from 6 K to 45 K results in a sharp decrease in adsorption amount from 35.78 mmol/g to just 0.03 mmol/g.

5. Conclusion

In this study, models of SWCNTs with varying diameters and inter-tube spacings were constructed. It was found that as the tube diameter increases, the specific surface area, porosity, and pore volume also increase. Similarly, increasing the inter-tube spacing leads to higher values of these structural parameters. The adsorption of ^{4}He on these SWCNT models was simulated across a pressure range up to 200 kPa using GCMC method, covering temperatures from the liquid helium to liquid nitrogen region. The simulation results show that at lower temperatures, the saturated adsorption capacity is significantly higher, and the pressure required to reach saturation is lower.

Acknowledgments
This work is supported by the China Postdoctoral Science Foundation (No. 2024M753312) and Tianjin Municipal Education Commission Scientific Research Program (No.2024KJ079).

References

[1] Xi X, Wang J, Chen L, Zhou Y and Wang J 2020 *J. Low. Tem. Phys.* **199** 1363-1381.
[2] Ozawa S, Kusumi S and Ogino Y 1976 *J. Colloid Interf. Sci.* **56(1)** 83-91.
[3] Hoffman C J, Edeskuty F J and Hammel E F 1956 *J. Chem. Phys.* **24(1)** 124-130.
[4] Xi X, Yang B, Wang J, Chen L and Wang J 2021 *J. Therm. Sci. Eng. Appl.* **13(5)** 051020.
[5] Salas-Guerrero L F, Builes S and Orozco G A 2024 *Int. J. Hydrogen Energ.* **50** 1626-1633.
[6] Sha H and Faller R 2016 *Comp. Mater. Sci.* **114** 160-166.
[7] Li S, Song K, Zhao D, Rugarabamu J R, Diao R and Gu Y 2020 *Micropor. Mesopor. Mat.* **302** 110220.
[8] Karki S and Chakraborty S N 2023 *Int. J. Hydrogen Energ.* **48(7)** 2731-2741.